Journal of Advanced College of Engineering and Management

Performance Assessment of Chirps, Persiann – CDR, IMERG, And TMPA Precipitation Products Across Nepal

Suraj Lamichhane[1], Nitesh Sharma[1], Nirajan Devkota*[1]

[1]Pulchowk Campus, Institute of Engineering, Tribhuvan University

*Email: 078phce112.nirajan@pcampus.edu.np

Abstract

The observation of hydrological as well as meteorological data is very essential for any kind of hydraulic and hydrological study. In Nepal, due to the significant variation of topography and climatic characteristics as well it is necessary to establish the meteorological stations densely, here only 231 meteorological stations are available and are handled by government organizations Department of Hydrology and Meteorology (DHM). Even though, due to many limitations, the satellite data is very useful for the water resources study. There are so many satellite products available but the performance of these products varies from place to place. In this study, the performance of four satellite products i.e., Climate Hazards Group Infrared Precipitation with Station data (CHIRPS), Precipitation Estimation from Remotely Sensed Information using Artificial Neural Networks (PERSIANN-CDR), Integrated Multi-Satellite Retrievals for GPM (IMERG), and TRMM Multi-satellite Precipitation Analysis (TMPA) all over Nepal are evaluated with different elevation bands. The performance of each product is evaluated by Probability of Detection (POD), Critical Success Index (CSI), Frequency Bias Index (FBI), False Alarm Ratio (FAR), Root Mean Square Error (RMSE), and Percentage Bias (PBIAS). After analysis of each product, the PERSIANN-CDR data set gives a reasonable performance for all elevation bands after bias correction.

Keywords: *Precipitation, Multi-satellite, Performance*

1. Introduction

Precipitation is integral to the Earth's hydrologic cycle, playing the foremost role in its water and energy balance. Accurate, uninterrupted, and uniform observation of precipitation represents an important input for hydrologic research and operational applications. In essence, the resilience and capacity of societies to react and adapt to climate extremes such as storms, floods, and droughts are greatly enhanced with a long-term historical record of precipitation. Practical applications include using precipitation intensity–duration–frequency (IDF) information for infrastructure design and developing early warning systems and disaster management planning by utilizing near-real-time precipitation data. Field-based rain gauge observations give reliable data locally even though the spatial distribution of rain gauge needs to be dense for good representation at the global scale. The use of satellite precipitation is another best way to study the high spatiotemporal variation of precipitation on a global scale [1].

In the complex topography of the Himalayan zone Nepal-like country and lack of rain gauge networks, employing satellite data is the best alternative way to study the mechanisms of precipitation systems. The data are juxtaposed with available field-based observed data to validate the accuracy of satellite measurements. A study by Kyaw et al. (2022) stated that there is an acceptable result between satellite and observed data for the intensity of 0.5 mm per hour.

After applying the Tropical Rainfall Measuring Mission (TRMM) satellite, satellite-based estimation techniques rose significantly, and various satellite product agencies and institutes provide satellite-based datasets, each derived using different algorithms. These products include the NOAA Climate Prediction Center (CPC) morphing technique CHORPH [3] NASA TRMM Multi-Satellite Precipitation Analysis (TMPA) [4] NASA Integrated Multi-Satellite Retrievals for GPM (IMERG)

[5], NRL – Blend Satellite Rainfall estimates from the Naval Research Laboratory (NRL) [6] and the Precipitation Estimation from Remotely Sensed Information using Artificial Neural Networks (PERSIANN) family products [7].

Different Satellite Precipitation Products (SPPs) show their effectiveness in different regions. In general, SPPs are strongly location-dependent. For example, TRMM, CHIRPS, MSWEP & PERSIANN-CDR show consistency with the ground-based precipitation in the mountain, Tibetan, and Himalayan regions. However, their products are not concisely examined in a well-performed hydrological model on the complex terrain, high elevation, and Himalayan regions of Nepal. TRMM was found superior in Karnali River Basin, and IMERG was superior in West Rapti Basin among various SPPs [8].

Due to the sparse distribution of hydro-meteorological stations and limitations of gauged observation, the results and interpretation of precipitation are further harmed by the discontinuity and missing values in meteorological data records. Hence newly developed SSPs could be used as an alternative to precipitation measurement in areas where stations are scarce [9]. Due to the lack of basin-wise hydrological data whether they are real-time or historical after management has been challenging [10]. Hence there is a need for a large-scale spatially distributed hydrological model forced with SPPs. In the context of Nepal, SPPs are barely used for hydrological application despite having SPPs driven hydrological model. With the ongoing advancement of SPPs, its hydrological application has also created a possible scope for the upcoming future. On the same basis, the objective of this study is to evaluate and quantify the effectiveness of SPPs and observed precipitation for reproducing hydrological conditions.

2. Materials and method

2.1 Study area

Nepal is a country in Asia, lying along the southern slopes of the Mountain ranges. Geographically located between India and China with 147181 square kilometers of area. Nepal occupies 0.3 and 0.03 percent of the land area of Asia and the world respectively. In the northern Hemisphere, Nepal is situated within latitudes 26º22’ N to 30º27’ N and of longitude 80º4’ to 88º12’ E. The altitude ranges from around 64 meters to 8848m above mean sea level. The country has a great variety of topography which is reflected in the diversity of weather and climate simultaneously. Especially, the country experiences tropical, mesothermal, micro thermal, taiga, and tundra type climatic regimes and precipitation patterns across the country. The average precipitation of Nepal is 1530 mm but they show huge variation from the south to north as well as east to west. There are two patterns of seasons summer and winter. The summer monsoon is further understood as pre-monsoon, monsoon, and post-monsoon. And again, Nepal is divided into five distinct physiographic zones: Terai, Siwaliks, Hills, Middle mountains, and High Mountains.

There are 4 main basins i.e., Koshi, Narayani, Karnali and Mahakali. They are snow-fed rivers and originated from large glaciers. Also, there are so many spring-fed and southern rivers. There are 51 discharge measurement stations along that river and 231 meteorological stations and all these gauging stations are operated by the Department of Hydrology and Meteorology. Among 231 meteorological stations, 74 stations lie below the elevation of 500m, 34 station lies between 500 and 1000m, 51 station lies between 2000 and 2500m, 10 station lies between 2500 and 3000m, 2 station lies between 3000 and 3500m and 2 station lies above 3500m as shown in Fig. 1. Due to complex topography and varying pattern of rainfall distribution, the rain gauge density is very low. And hence there is not a good representation of rainfall for quantifying it.

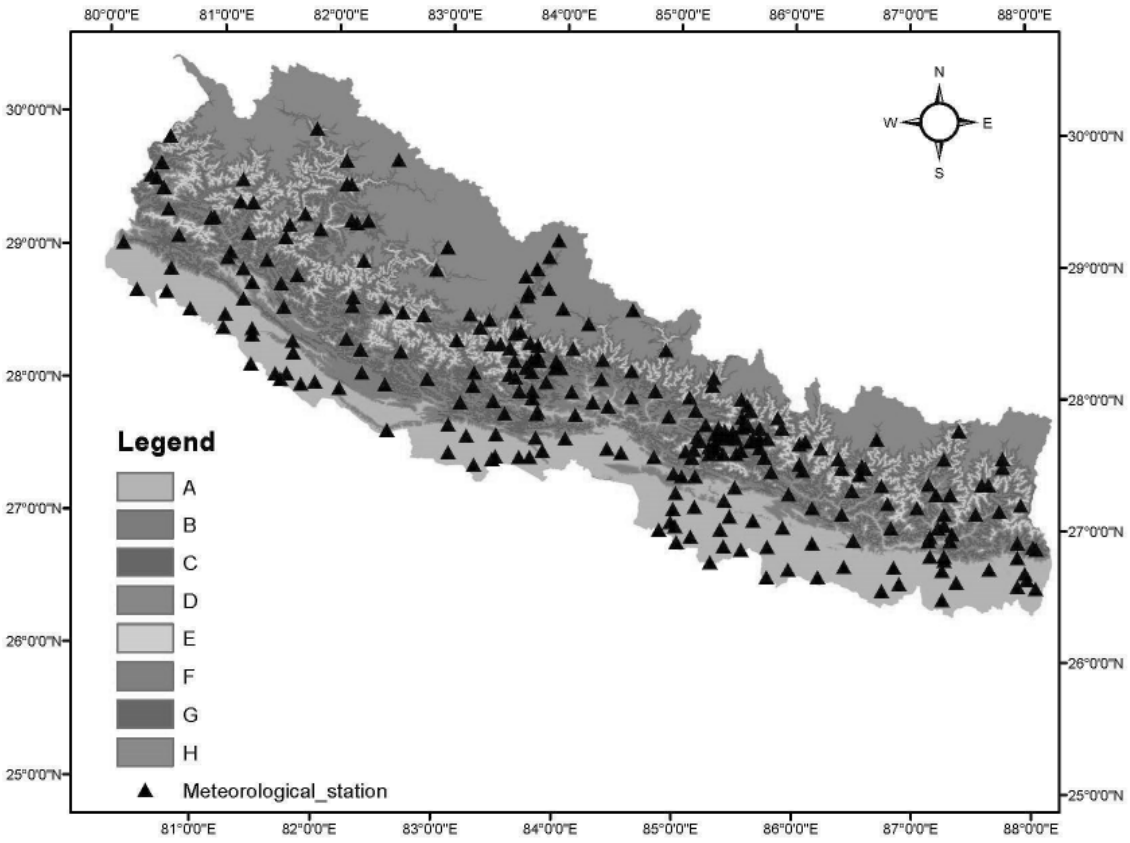

Figure 1: Study area with elevation band and meteorological stations

2.2 Description of the precipitation data set

Satellite Precipitation Products provide complementary information to the in-situ measurement for streamflow simulations to better understand the hydrological response (Khotakho et. Al., 2021). SPPs provide potential alternatives for maintaining precipitation on regular high–resolution grids, yielding an unprecedented level of detail, especially over remote areas and mountainous regions where stations are very sparse (Tamrakar et. Al. 2013). They are available on different spatial and temporal scales, in spatial (global and regional varying from $0.1^o \times 0.1^o$ to $1^o \times 1^o$) and in temporal (Half-hourly, hourly, daily, and monthly). Several SPPs employ different algorithms; some are available at a higher resolution but with less accuracy, whereas some are more accurate, but the resolution is coarse. There are several SPPs readily available to estimate the precipitation value by a multi-satellite approach.

S. No.	Data Type	Source	Spatial Resolution
1.	**CHIRPS**	https://data.chc.ucsb.edu/products/CHIRPS-2.0/.	$0.05^o \times 0.05^o$
2.	**PERSIANN-CDR**	http://chrsdata.eng.uci.edu/	$0.025^o \times 0.025^o$
3.	**IMERG**	https://gpm.nasa.gov/data/sources	$0.1^o \times 0.1^o$
4.	**TMPA**	https://disc.gsfc.nasa.gov/datasets/TRMM_3B42_7/summary	$0.025^o \times 0.025^o$

i. CHIRPS

The CHIRPS data combine the TIR satellite observations, atmospheric model rainfall fields from the NOAA) National Oceanic and Atmospheric Administration) Climate Forecast System, version 2 (CFSv2), Climate Hazards Precipitation Climatology (CHPClim), the TRMM 3B42 product from National Aeronautics Space Agency (NASA), and in situ rainfall observations from national and regional meteorological services. The CHIRPS product is a high-resolution (0.05°) rainfall dataset developed by the US Geological Survey (USGS) and the Climate Hazards Group at the University of California, Santa Barbara, available at https://data.chc.ucsb.edu/products/CHIRPS-2.0/.

For any given pixel, the CHIRPS blending procedure is based on a weighted average of the ratios between the five closest stations and the CHIRPS: b1.5=(s1..5+ε)/(c1..5+ε), where b is a 5-element vector of bias ratios, s is a 5 element vector of station observations, c is a 5-element vector of CHIRP values. A small epsilon number (ε) is included in the denominator and numerator to handle zero or near zero CHIRP values. The ratios greater than three are capped at three. Bias values (b) for any station beyond the decorrelation distance are assumed to be 1.

A weighted average of these five bias values is then calculated, based on their distances and the decorrelation slope described above. A further calculation adjusts this value based on the expected correlation with the nearest station (Rns) and the expected correlation between 'true' precipitation values and the CHIRP data (RCHIRP). RCHIRP is set a priori at 0.5 based on validation results. These correlations are used to assign a weighting value for the CHIRP: α=RCHIRP/(RCHIRP+Rns). The final CHIRPS estimate is a combination of unadjusted and bias-adjusted CHIRP data: CHIRPS=αCHIRP+(1-α)bCHIRP. Thus, even in the presence of co-located stations, the CHIRPS will have some influence from the CHIRP.

ii. PERSIANN-CDR

The PERSIANN algorithm is an artificial neural network (ANN) model based on a multilayer neural feed forward network (MFN) known as the Modified Counter Propagation Network[7]. This hybrid model consists of two processes. First, the infrared (10.2–11.2 μm) images are transformed into the hidden layer through an automatic clustering process to form what is known as a self-organizing feature map (SOFM). The purpose of this process is to detect and classify patterns in the input data. Then, the discrete SOFM clusters in the hidden layer are mapped to the continuous space of outputs (i.e., rainfall rate). Both processes of input-hidden and hidden-output transformations involve parameter estimation, which is routinely performed by incorporating passive microwave (PMW) rainfall from low Earth orbiting satellites. It is noteworthy that parameter estimation in each process can be performed separately by training the model for the former while a supervised learning strategy is used for the latter. PERSIANN data are available for public use through the CHRS Data Portal at http://chrsdata.eng.uci.edu (last access: 8 November 2018). For a comprehensive description of the PERSIANN-CDR algorithm, interested readers should refer to [11].

iii. IMERG

IMERG is a gridded precipitation product that merges measurements from a network of satellites in the GPM constellation. IMERG uses the GPM Core Observatory satellite, which has a dual-frequency precipitation radar and a 13-channel passive microwave imager, as a reference standard

to intercalibrate and merge precipitation estimates from individual passive microwave (PMW) satellites in the constellation.

IMERG has a high resolution of 0.1° every half-hour covering up to ±60° latitudes. Three choices of IMERG runs are available depending on user requirements. The Early Run, available at a 6-h delay for real-time applications such as hazard predictions, is limited to rainfall morphing only forward in time. The Late Run, with an 18-h delay for purposes such as crop forecasting, employs morphing both forward and backward in time. The Final Run is at a 4-month delay for research applications. Both the Early and Late Runs have climatological gauge adjustment while the Final Run uses monthly gauge adjustments to reduce bias. Moreover, runs with longer delays will use more PMW estimates because of latency in data delivery. Note that these delays will eventually be reduced toward the targets of 4 h, 12 h, and 2 months, respectively. This study focuses on the calibrated estimate from the Final Run of IMERG, which is available from April 2014 onward.

This algorithm is particularly valuable over the majority of the Earth's surface that lacks precipitation-measuring instruments on the ground. Now in the latest Version 06 release of IMERG the algorithm fuses the early precipitation estimates collected during the operation of the TRMM satellite (2000 - 2015) with more recent precipitation estimates collected during operation of the GPM satellite (2014 - present). The longer the record, the more valuable it is, as researchers and application developers will attest. By being able to compare and contrast past and present data, researchers are better informed to make climate and weather models more accurate, better understand normal and extreme rain and snowfall around the world, and strengthen applications for current and future disasters, disease, resource management, energy production and food security.

iv. TMPA

TMPA (also known as TRMM 3B42) is the gridded precipitation product from the TRMM project. Just as with IMERG, TMPA uses the TRMM satellite to calibrate and combine PMW estimates from different platforms. Estimates derived from geosynchronous IR measurements calibrated against PMW estimates on a monthly basis are used to fill in the gaps in the PMW field.

TMPA is available at a resolution of 0.25° every 3 h covering up to ±50° latitudes. Two different products of TMPA are available: the real-time product (with a 9-h delay) and the research product. This study uses the research product, which is available beginning in 1998. The research product utilizes the TRMM Precipitation Radar onboard the satellite for calibration and has the additional monthly gauge adjustment step.

The combination of satellite-borne passive and active sensors to be deployed in the upcoming TRMM promises to provide critical information regarding the three-dimensional distributions of precipitation and heating in the Tropics (Simpson et al. 1996). Coincident measurements from TMI and PR are complementary: passive microwave radiometers measure radiances that are the end product of the integrated effects of electromagnetic absorption–emission and scattering through the precipitating cloud along the sensor view path. The frequency dependence of electromagnetic properties of cloud and precipitation particles allows for the design of multichannel passive microwave radiometers that can ‘‘sound’’ to different depths in a precipitating cloud, but the height assignment of cloud properties is not very specific. On the other hand, active microwave sensors (radars) provide specific height information based upon the time delay of the precipitation-backscattered return power. However, simple one-parameter radars

(such as the TRMM PR) only operate at one transmitting/receiving frequency and polarization. To obtain unambiguous precipitation water content profiles from these radars, secondary signal effects such as path attenuation must be determined independently. The VIRS on TRMM adds cloud-top temperatures and structures to complement the description of the two microwave sensors. While direct precipitation information from VIRS is less reliable than that obtained by the microwave sensors, VIRS serves an important role as a bridge between the high quality but infrequent observations from TMI and PR with the more available data and longer time series data available from the geostationary VIS/IR satellite platforms. The CERES and the LIS, while designated as EOS instruments, still play an important role in the TRMM mission to round out the scientific objectives. The lightning sensor Goodman & Christian, (1993) aside from mapping the global frequency of lightning events, will play an important role in coupling the occurrence of lightning to the precipitation—thus enhancing our overall understanding of both lightning as well as precipitation processes. The CERES instrument [13] allows for determination of the total radiant energy balance. Together with the latent heating derived from the precipitation, a significantly improved picture of the atmospheric energy system can emerge. A substantial number of recent scientific publications have dwelled upon the importance of TRMM, the development of rainfall algorithms, and the applications of TRMM data. The focus of this paper is on the measurements that will be made by the TRMM rainfall sensors. The subsequent sections describe each of the three primary rainfall instruments, their measurement characteristics, their scanning geometry, and their expected data products.

3 Methodology

The general methodological flowchart of the work to be performed under this research is shown in Fig. 2. The methodology starts with the extraction of required SPPs data from the earth engine, then compares the raw data for SPPs with gauged observations which are available from the Department of Hydrology and Meteorology (DHM) and perform a quantitative evaluation. For correcting systematic biases present in SPPs data to conserve the volume of precipitation empirical robust technique was used. After correcting biases, suitable sets of SPPs are recommended for various regions of Nepal.

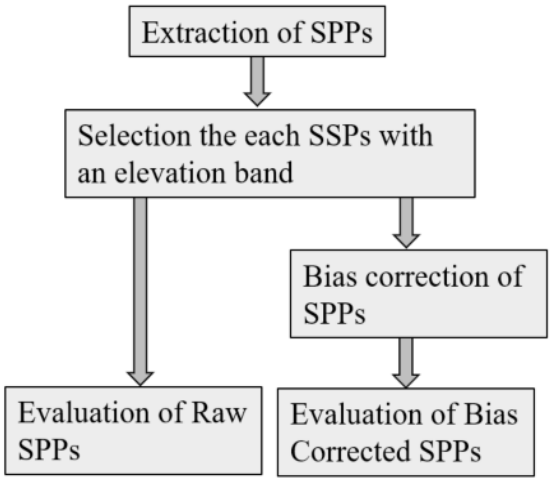

Figure 2: Overall Methodological Framework

3.1 Extraction of SPPs

Different SPPs data are available in various sources but in this study, SPPs data were extracted from the earth engine. The earth engine [https://developers.google.com/earth-engine/datasets/] is a platform

for scientific analysis and visualization of geospatial datasets, for academic, non-profit, business, and government users. Earth engine hosts satellite imagery and stores it in a public data archive that includes historical earth images going back more than forty years. The images, ingested daily, are then made available for global-scale data mining. Earth engine also provides other tools to enable the analysis of large datasets.

A streamlined framework design of the earth engine is shown in Fig 3. Code editor of earth engine and third-party applications use client libraries to send interactively or batch queries to the system through REST API. Front End servers handle on-the-fly requests. It also forwards complex sub-queries to Computer Masters which manage the process among a pool of Computer Servers. Batch computation does the same. Backing both computation systems is a collection of data services, including an Asset Database that contains the per image metadata and provides efficient capabilities [14].

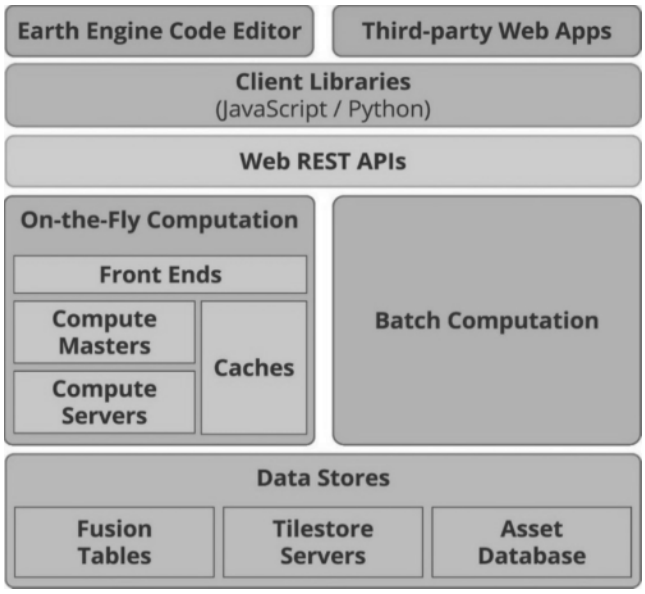

Figure 3: System architecture of earth engine

a. Bias correction of SPPs

Raw SPPs are supposed to have random biases. So, before evaluation of SPPs, they are subjected to bias correction. For bias correction of raw SPPs, the robust quantile mapping method was applied. The robust quantile mapping method for the bias correction was performed using R-studio software 2020 [15]. During bias correction to avoid the seasonality effect, firstly each year's monthly data was segregated from the whole data and bias correction for the individual month was done. Later, all data was again aggregated into daily form after monthly bias correction.

b. Evaluation of SPPs

Evaluation of SPPs has been done based on six indices i.e., Probability of Detection (POD), Critical Success Index (CSI), Frequency Bias Index (FBI), False Alarm Ratio (FAR), Root Mean Square Error (RMSE), and Percentage Bias (PBIAS). Among these six indices, the earlier four are performance-based indices and the last two are magnitude-based indices.

In the case of performance-based indices, this study carried out the comparison between SSPs concerning different rain gauge observations. The extreme precipitation detection is "True" when both SPPs and rain gauge observations show a daily rainfall ≥ 1mm while it is "False" when both SPPs

detect rain during non-rainy days based on rain-gauge observations. Similarly, the extreme precipitation detection is "Miss" when SPPs and rain gauge observations show a daily rainfall<1mm. Based on the total count of these detections, four indices POD, CSI, FAR, and FBI were calculated as follows:

$$(1)\ \mathrm{POD} = \frac{\mathrm{True}}{\mathrm{True} + \mathrm{Miss}}$$

$$(2)\ \mathrm{CSI} = \frac{\mathrm{True}}{\mathrm{True} + \mathrm{Miss} + \mathrm{False}}$$

$$(3)\ \mathrm{FAR} = \frac{\mathrm{False}}{\mathrm{True} + \mathrm{False}}$$

$$(4)\ \mathrm{FBI} = \frac{\mathrm{True} + \mathrm{False}}{\mathrm{True} + \mathrm{Miss}}$$

POD shows the proportion of how well precipitation events are detected compared to that of total gauged-based precipitation events. CSI shows the overall proportion of how well precipitation events are detected compared to that of the total number of precipitation events detected either by gauge or satellite. The FAR for precipitation detection is the number of false precipitation detection per total number of precipitation detection FBI shows a biasness between gauge precipitation and satellite detected precipitation based on frequency.

POD, CSI, and FAR values range from 0-1. Higher values are preferred for POD and CSI whereas lower values are preferred for FAR but not at a cost of under-reporting actual danger. The value of FBI ranges from 0 to ∞. FBI value lesser than 1 implies the underestimation of precipitation events detection whereas a value greater than 1 implies the overestimation of precipitation events detection.

In the case of magnitude-based indices, PBIAS and RMSE were computed for selected SPPs concerning gauged rain gauge observation.

Percentage Bias measures the average tendency of the simulated data to be larger or smaller than their observed counterparts Moriasi et al. (2015) the optimal value of PBIAS is 0, with low-magnitude values indicating accurate model simulation. Positive values indicate model underestimation bias, and negative values indicate model overestimation bias [17].

Root mean square error (RMSE): RMSE provides information about the performance of SPPs by allowing a comparison of differences between the SPPs value and gauge value. The smaller value of RMSE indicates better performance of SPPs data. Considering its limitation, a few large errors in the sum may significantly increase RMSE.

c. Classification of SPPs

As per the obtained value of six indices i.e., POD, CIS, FAR, RMSE, and PBIAS all the SPPs were classified for various regions of Nepal Based on the elevation bands. Seven bands are assigned for 231-gauge stations based on the elevation range. The assigned bands are presented in Table 1.

Table 1: Elevation band with elevation

Elevation Band	Elevation Range
A	≤ 500m
B	500-1000m
C	1000-1500m
D	1500-2000m
E	2000-2500m
F	2500-3000m
G	3000-3500m
H	≥ 3500m

4. Results and discussion

The Google earth engine has been used to extract the SPPs data freely. And it was evaluated based on performance and magnitude-based indices. The results of evaluations of different candidate raw and bias-corrected SPPs are presented in Table 2 and Table 3 respectively. Here, in the case of Raw SPP, for each elevation band, the value of RMSE and PBIAS have higher values, and the higher value of FAR shows no products providing good results. And again, for the bias-corrected data of each product and in each elevation band the lower value of RMSE and PBIAS mainly and lower value of FAR as well as the higher value of POD and CSI show that PERSIANN -CDR SPPs give good results.

Table 2: Raw SPP indices for all elevation band

SPPs	POD	CSI	FAR	FBI	RMSE	PBIAS	Elevation band
CHIRPS	0.456	0.301	0.525	0.983	19.22	5.15	A
IMERG	0.332	0.16	0.761	1.436	24.84	7.31	
PERSIANN	0.751	0.38	0.563	1.773	262.19	132.44	
TRMM	0.269	0.131	0.797	1.354	25.04	4.83	
CHIRPS	0.3871	0.275	0.499	0.796	15.15	-23.97	B
IMERG	0.346	0.187	0.706	1.233	13.08	-9	
PERSIANN	0.734	0.4	0.524	1.581	261.79	218.89	
TRMM	0.287	0.152	0.755	1.232	14.52	-27.93	

CHIRPS	0.3607	0.266	0.484	0.72	13.39	-38.31	C
IMERG	0.369	0.203	0.684	1.225	14.63	-40.75	
PERSIANN	0.718	0.412	0.506	1.492	261.75	213.26	
TRMM	0.315	0.168	0.733	1.221	15.94	-63.18	
CHIRPS	0.3419	0.264	0.452	0.72	20.36	16.91	D
IMERG	0.362	0.212	0.657	1.103	24.6	12.75	
PERSIANN	0.712	0.425	0.482	1.415	262.25	136.33	
TRMM	0.323	0.183	0.702	1.13	25.46	-0.5	
CHIRPS	0.2875	0.229	0.466	0.547	13.75	12.4	E
IMERG	0.343	0.206	0.656	1.022	13.96	7.66	
PERSIANN	0.64	0.399	0.485	1.263	261.78	191.98	
TRMM	0.306	0.176	0.705	1.062	13.93	10.01	
CHIRPS	0.2674	0.204	0.506	0.594	15.9	36.03	F
IMERG	0.327	0.187	0.681	1.171	14.08	53.76	
PERSIANN	0.635	0.347	0.552	1.603	261.851	169.319	
TRMM	0.308	0.169	0.722	1.252	15.89	21.41	
CHIRPS	0.2539	0.207	0.471	0.48	12	22.08	G
IMERG	0.318	0.193	0.668	0.957	10.87	29.42	
PERSIANN	0.563	0.363	0.493	1.114	261.75	226.975	
TRMM	0.311	0.181	0.697	1.028	10.81	36.94	
CHIRPS	0.2803	0.21	0.543	0.613	10.61	-74.73	H
IMERG	0.305	0.172	0.714	1.061	8.1	-70.6	
PERSIANN	0.644	0.348	0.568	1.493	261.656	324.33	
TRMM	0.283	0.157	0.733	1.036	9.18	-91.39	

Table 3: Bias Corrected SPP indices for all elevation band

SPPs	POD	CSI	FAR	FBI	RMSE	PBIAS	Elevation band
CHIRPS	0.712	0.311	0.642	2.016	21.85	-14.69	
IMERG	0.468	0.286	0.585	1.112	24.9	-0.8	A
PERSIANN	0.493	0.331	0.503	0.995	21.57	-0.18	
TRMM	0.726	0.364	0.578	1.748	24.91	-6.2	
CHIRPS	0.846	0.398	0.572	2.021	12.27	-20.58	
IMERG	0.580	0.371	0.504	1.164	12.82	-1.63	B
PERSIANN	0.536	0.373	0.457	0.990	12.5	-0.17	
TRMM	0.701	0.405	0.516	1.467	12.85	-8.18	
CHIRPS	0.862	0.400	0.572	2.082	9.69	-29.25	
IMERG	0.602	0.394	0.478	1.149	10.55	-0.48	C
PERSIANN	0.557	0.390	0.444	1.003	10.09	-0.12	
TRMM	0.709	0.429	0.485	1.387	10.39	-9.34	
CHIRPS	0.897	0.420	0.558	2.103	22.65	-12.35	
IMERG	0.632	0.426	0.447	1.139	24.24	-2.86	D
PERSIANN	0.592	0.425	0.412	1.006	23.06	-0.3	
TRMM	0.746	0.464	0.453	1.387	23.81	-6.58	
CHIRPS	0.913	0.408	0.574	2.200	10.56	-24.41	
IMERG	0.636	0.424	0.450	1.159	11.12	-3.23	E
PERSIANN	0.592	0.416	0.422	1.029	10.94	-0.29	
TRMM	0.697	0.444	0.457	1.286	11.35	-5.33	
CHIRPS	0.787	0.352	0.621	2.095	12.23	-26.78	
IMERG	0.542	0.369	0.516	1.101	12.89	-2.82	F
PERSIANN	0.560	0.392	0.470	1.047	12.53	-3.72	

TRMM	0.592	0.382	0.523	1.228	13.25	-3.89	
CHIRPS	0.894	0.410	0.566	2.086	10.63	-35.6	G
IMERG	0.609	0.406	0.449	1.108	10.51	-2.93	
PERSIANN	0.617	0.428	0.415	1.059	10.82	-2.73	
TRMM	0.684	0.439	0.448	1.241	11.3	-5.81	
CHIRPS	0.779	0.353	0.612	2.040	5.21	-30.89	H
IMERG	0.536	0.330	0.537	1.159	5.52	-1.83	
PERSIANN	0.489	0.325	0.507	0.992	5.23	-0.25	
TRMM	0.613	0.362	0.529	1.302	5.57	-3.36	

From the result above, it can be seen that the raw data have lower values of CSI, POD, and higher values of FAR, FBI, RMSE, and PBIAS. Using raw data directly for hydrological models, therefore, seems unlikely. But, after bias correction of raw data using empirical robust quantile mapping method, it is seen that the performance of each SPP is highly improved in terms of performance-based indices and is not greatly influenced in terms by magnitude-based indices. Therefore, for the hydrological model using bias-corrected SPP data seems likely to get better results.

Looking as a whole, bias-corrected PERSIANN-CDR showed a good result amongst other candidates' SPPs in all elevation bands, POD and CSI were quite good compared to another candidate SPPs. FAR was also low compared to other SPPs. In every elevation band, the value of FBI for PERSIANN-CDR was nearly equal to 1 which means a good estimation of precipitation events. RMSE was lower for PERSIANN-CDR for all elevation bands and nearly equal to unity which implies a slight overestimation in terms of magnitude. Overall, PERSIANN-CDR was found most suitable alternative to other candidate SPPs for all elevation bands.

3. Conclusion

This study evaluated different candidate SPPs based on performance and magnitude-based indices and applied the results to classify different SPPs for the various region in Nepal based on elevation bands. The key conclusions from this study are as follows:

- The value of POD and CSI was found quite good for bias-corrected PERSIANN-CDR as compared to another candidate SPPs for various regions of Nepal. Also, the FAR value was low and FBI was near equal to 1 which implied a good estimation of precipitation events.
- The value of RMSE for all elevation bands for bias-corrected PERSIANN-CDR was found lower compared to another candidate SPPs. Also, the value of PBIAS was found negative and nearly equal to 1 which implied a slight overestimation of the magnitude of precipitation.
- Considering, the values of all the indices computed, PERSIANN-CDR was found good for all elevation bands compared to other candidate SPPs.
- Hourly-based products yield irrational results and don't seem quite useful in analysis.

References:

[1] P. Nguyen *et al.*, "Global Precipitation Trends across Spatial Scales Using Satellite Observations," *Bull. Am. Meteorol. Soc.*, vol. 99, no. 4, pp. 689–697, 2018, doi: 10.1175/BAMS-D-17-0065.1.

[2] A. K. Kyaw, S. Shahid, and X. Wang, "Remote Sensing for Development of Rainfall Intensity–Duration–Frequency Curves at Ungauged Locations of Yangon, Myanmar," *Water (Switzerland)*, vol. 14, no. 11, 2022, doi: 10.3390/w14111699.

[3] R. J. Joyce, J. E. Janowiak, P. A. Arkin, and P. Xie, "CMORPH: A Method that Produces Global Precipitation Estimates from Passive Microwave and Infrared Data at High Spatial and Temporal Resolution," *J. Hydrometeorol.*, vol. 5, no. 3, pp. 487–503, 2004, doi: 10.1175/1525-7541(2004)005<0487:CAMTPG>2.0.CO;2.

[4] G. J. Huffman, R. F. Adler, D. T. Bolvin, and E. J. Nelkin, "The TRMM Multi-Satellite Precipitation Analysis (TMPA) BT - Satellite Rainfall Applications for Surface Hydrology," M. Gebremichael and F. Hossain, Eds. Dordrecht: Springer Netherlands, 2010, pp. 3–22. doi: 10.1007/978-90-481-2915-7_1.

[5] T. Ushio *et al.*, "A Kalman filter approach to the Global Satellite Mapping of Precipitation (GSMaP) from combined passive microwave and infrared radiometric data," *J. Meteorol. Soc. Japan. Ser. II*, vol. 87, pp. 137–151, 2009.

[6] F. J. Turk and S. D. Miller, "Toward improved characterization of remotely sensed precipitation regimes with MODIS/AMSR-E blended data techniques," *IEEE Trans. Geosci. Remote Sens.*, vol. 43, no. 5, pp. 1059–1069, 2005.

[7] K. Hsu, X. Gao, S. Sorooshian, and H. V Gupta, "Precipitation estimation from remotely sensed information using artificial neural networks," *J. Appl. Meteorol.*, vol. 36, no. 9, pp. 1176–1190, 1997.

[8] R. Talchabhadel *et al.*, "Evaluation of precipitation elasticity using precipitation data from ground and satellite-based estimates and watershed modeling in Western Nepal," *J. Hydrol. Reg. Stud.*, vol. 33, p. 100768, 2021, doi: https://doi.org/10.1016/j.ejrh.2020.100768.

[9] D. M. Moges, A. Kmoch, and E. Uuemaa, "Application of satellite and reanalysis precipitation products for hydrological modeling in the data-scarce Porijõgi catchment, Estonia," *J. Hydrol. Reg. Stud.*, vol. 41, p. 101070, 2022, doi: https://doi.org/10.1016/j.ejrh.2022.101070.

[10] A. H. M. Siddique-E-Akbor *et al.*, "Satellite Precipitation Data–Driven Hydrological Modeling for Water Resources Management in the Ganges, Brahmaputra, and Meghna Basins," *Earth Interact.*, vol. 18, no. 17, pp. 1–25, 2014, doi: 10.1175/EI-D-14-0017.1.

[11] H. Ashouri *et al.*, "PERSIANN-CDR: Daily precipitation climate data record from multisatellite observations for hydrological and climate studies," *Bull. Am. Meteorol. Soc.*, vol. 96, no. 1, pp. 69–83, 2015.

[12] S. J. Goodman and H. J. Christian, "Global observations of lightning," *Atlas Satell. Obs. Relat. to Glob. Chang.*, vol. 191, p. 219, 1993.

[13] B. A. Wielicki, B. R. Barkstrom, E. F. Harrison, R. B. Lee III, G. L. Smith, and J. E. Cooper, "Clouds and the Earth's Radiant Energy System (CERES): An earth observing system experiment," *Bull. Am. Meteorol. Soc.*, vol. 77, no. 5, pp. 853–868, 1996.

[14] N. Gorelick, M. Hancher, M. Dixon, S. Ilyushchenko, D. Thau, and R. Moore, "Google Earth Engine: Planetary-scale geospatial analysis for everyone," *Remote Sens. Environ.*, vol. 202, pp. 18–27, 2017.

[15] H. Wickham *et al.*, "RStudio (2020)," *Dplyr A Gramm. Data Manip.*.

[16] D. N. Moriasi, M. W. Gitau, N. Pai, and P. Daggupati, "Hydrologic and water quality models: Performance measures and evaluation criteria," *Trans. ASABE*, vol. 58, no. 6, pp. 1763–1785, 2015.

[17] H. V. Gupta, S. Sorooshian, and P. O. Yapo, "Status of automatic calibration for hydrologic models: Comparison with multilevel expert calibration," *J. Hydrol. Eng.*, vol. 4, no. 2, pp. 135–143, 1999.